Title

Activity-dependent regulation of Cdc42 by Ephexin5 drives synapse growth and stabilization

Journal

Science Advances, 11(13)

ISSN

2375-2548

Authors

Petshow, Samuel

Coblentz, Azariah

Hamilton, Andrew M

et al.

Publication Date

2025-03-28

DOI

10.1126/sciadv.adp5782

Peer reviewed

CELLULAR NEUROSCIENCE

Activity-dependent regulation of Cdc42 by Ephexin5 drives synapse growth and stabilization

Samuel Petshow, Azariah Coblentz, Andrew M. Hamilton, Dipannita Sarkar, Margarita Anisimova, Juan C. Flores, Karen Zito*

Synaptic Rho guanosine triphosphatase (GTPase) guanine nucleotide exchange factors (RhoGEFs) play vital roles in regulating the activity-dependent neuronal plasticity that is critical for learning. Ephexin5, a RhoGEF implicated in the etiology of Alzheimer's disease and Angelman syndrome, was originally reported in neurons as a RhoA-specific GEF that negatively regulates spine synapse density. Here, we show that Ephexin5 activates both RhoA and Cdc42 in the brain. Furthermore, using live imaging of GTPase biosensors, we demonstrate that Ephexin5 regulates activity-dependent Cdc42, but not RhoA, signaling at single synapses. The selectivity of Ephexin5 for Cdc42 activation is regulated by tyrosine phosphorylation, which is regulated by neuronal activity. Last, in contrast to Ephexin5's role in negatively regulating synapse density, we show that, downstream of neuronal activity, Ephexin5 positively regulates synaptic growth and stabilization. Our results support a model in which plasticity-inducing neuronal activity regulates Ephexin5 tyrosine phosphorylation, driving Ephexin5-mediated activation of Cdc42 and the spine structural growth and stabilization vital for learning.

INTRODUCTION

The activity-dependent growth and retraction of dendritic spines and their associated synapses is a vital component of the neural circuit plasticity that occurs during learning (*1*–*4*). The Rho guanosine triphosphatases (GTPases) RhoA, Cdc42, and Rac1 are important regulators of the spine actin cytoskeleton, and their activation in dendritic spines is required for the structural and functional changes in spine synapses that support learning (*5*–*10*). While spine structural plasticity relies on the coordinated action of all three of these Rho GTPases, each plays a functionally and spatiotemporally distinct role in spine remodeling (*8*, *11*, *12*). Indeed, RhoA activation leads to actomyosin contraction, driving spine shrinkage and retraction, while Cdc42 activation leads to actin nucleation and polymerization, driving spine growth and stabilization (*7*, *11*–*16*). Thus, precise control over the activation of each GTPase is crucial for the activity-dependent plasticity that supports learning.

GTPase activation is tightly and precisely regulated by Rho GTPase guanine nucleotide exchange factors (RhoGEFs) and Rho GTPase activating proteins (RhoGAPs). RhoGEFs catalyze exchange of guanosine diphosphate (GDP) for guanosine triphosphate (GTP), converting the GTPase from its inactive, GDP-bound state to its active, GTP-bound state, whereas RhoGAPs deactivate GTPases through stimulating hydrolysis of GTP to GDP (*12*, *17*). Ephexin5 (E5) is a RhoGEF that was identified as a negative regulator of spine synapse density and outgrowth (*18*–*21*). Initial work in whole brain tissue and vascular smooth muscle cells identified E5 as RhoA-specific GEF (*18*, *22*). Notably, E5 activation of RhoA in the brain is thought to be important for its role in contributing to amyloid-β (Aβ)-induced spine loss in neurons (*20*) and memory deficits seen in mouse models for Alzheimer's disease (*23*, *24*).

Most studies on brain E5 highlight its role in restricting synapse density and spine outgrowth; in contrast, downstream of neuronal activation, E5 has been implicated in promoting spine outgrowth (*19*). Furthermore, in mouse models of Angelman syndrome, E5 was reported to mediate an increase in spine density (*25*). It has been unclear how these diverse roles of E5, often with opposing outcomes on spine synapse structure, are carried out by the same molecule. Intriguingly, studies in nonneuronal cells have asserted that E5 can contribute to the activation of Cdc42 (*26*, *27*). In addition, several studies report that both the activation and substrate selectivity of RhoGEFs can be regulated by phosphorylation (*28*–*30*). Therefore, we hypothesized that the spine stabilizing role of E5 is regulated by an activity- and phosphorylation-dependent mechanism, driving Cdc42 activation and facilitating activity-dependent spine outgrowth.

Here, we demonstrate in brain tissue that E5 regulates not only RhoA but also Cdc42. Furthermore, using live-cell imaging of Förster resonance energy transfer (FRET)–based GTPase biosensors at single synapses, we show that E5 regulates the activation of Cdc42, but not RhoA, during plasticity that drives long-term synaptic growth and strengthening. We further find that neuronal plasticity is accompanied by a reduction in levels of tyrosine-phosphorylated E5 and that a mutation of a key tyrosine residue on E5, Y361, enhances E5-dependent activation of Cdc42. Last, we demonstrate that E5 GEF activity is required for activity-dependent long-term spine growth and Cdc42 signaling. Together, our results support a model in which potentiating synaptic plasticity drives dephosphorylation of E5, directing E5 substrate selectivity toward the activation of Cdc42, a vital step in the activity-dependent spine structural plasticity that supports learning.

RESULTS

Activation of both Cdc42 and RhoA is reduced in E5KO brains

To test our hypothesis that E5 plays a role in the activation of both RhoA and Cdc42 in brain tissue, we measured levels of active RhoA and Cdc42 in E5 knockout (E5KO) and wild-type (WT) whole mouse brains using an active GTPase pull-down assay (*31*). In this assay, active GTP-bound GTPases are isolated from samples via their interaction with the GTPase-binding domain of a downstream effector protein [Rhotekin for RhoA and p21-activated protein

Center for Neuroscience, University of California, Davis, Davis, CA 95618, USA.
*Corresponding author. Email: kzito@ucdavis.edu

kinase (PAK) for Cdc42] and detected following SDS–polyacrylamide gel electrophoresis (SDS-PAGE) via immunoblot.

We measured active RhoA and Cdc42 levels from the brains of postnatal day 19 (P19) to P21 E5KO mice and WT littermates. Consistent with previous findings in brain and human embryonic kidney (HEK) 293T cells (*18*, *22*, *26*), we found that active RhoA levels were reduced in E5KO brains compared to WT littermates (Fig. 1, A and B; E5KO/WT, 0.72 ± 0.05). Notably, we also found that active Cdc42 levels were reduced to a similar extent in E5KO brains compared to WT littermates (Fig. 1, C and D; E5KO/WT, 0.71 ± 0.09). We conclude that E5 regulates the activity of both RhoA and Cdc42 in the brain.

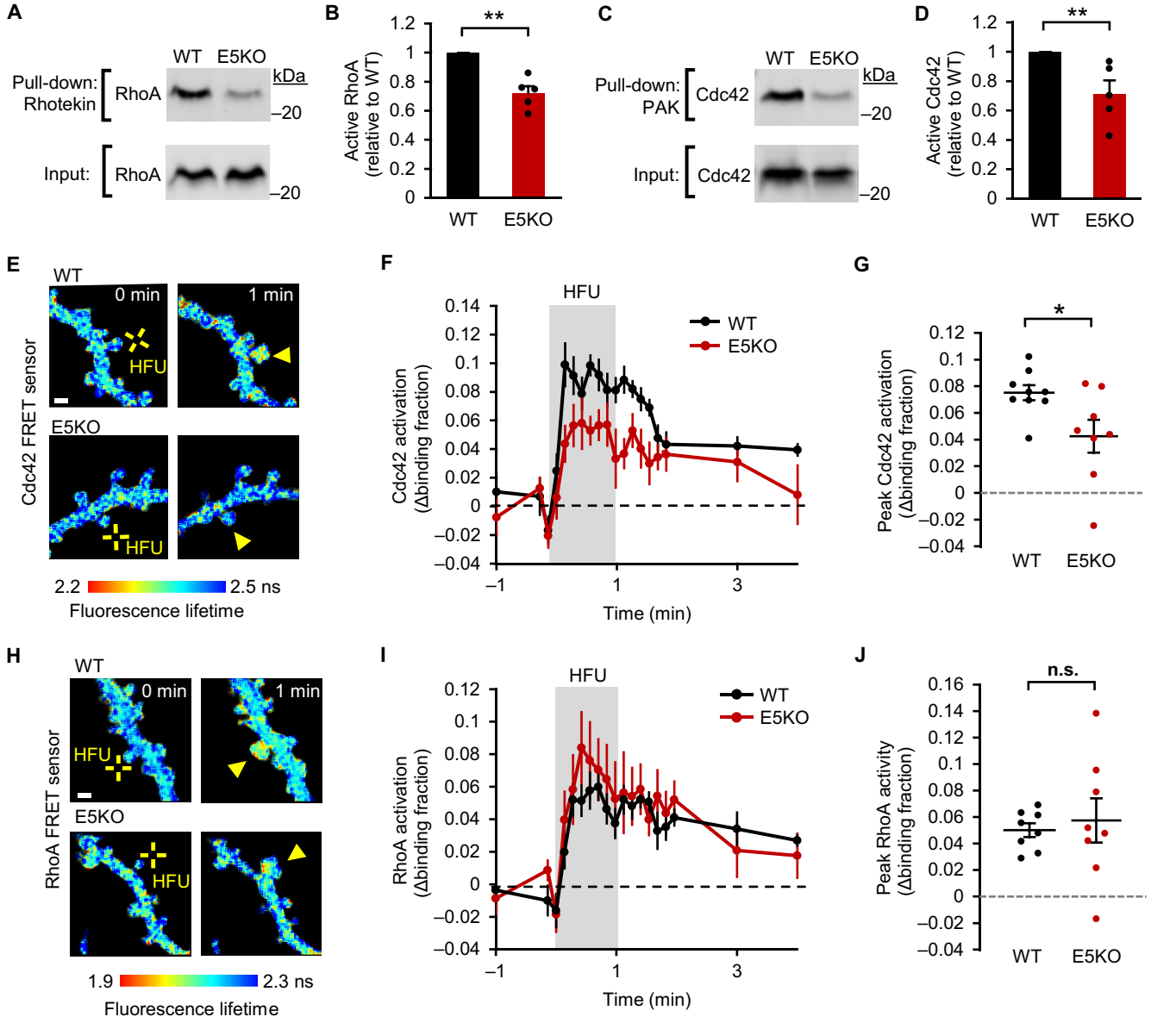

Fig. 1. Activity-dependent Cdc42, but not RhoA, signaling is regulated by E5. (**A**) Immunoblot showing active RhoA (Rhotekin pull-down), isolated from whole brain lysates (input) of P18 to P21 E5KO or WT littermate mice. (**B**) Active RhoA signal/total RhoA signal normalized to WT is reduced in E5KO brains (red; 5 brains) relative to WT littermates (black; 5 brains). (**C**) Immunoblot showing active Cdc42 (PAK pull-down), isolated from whole brain lysates (input) of P18 to P21 E5KO or WT littermates. (**D**) Active Cdc42 signal/total Cdc42 signal and normalized to WT is reduced in E5KO brains (red; 5 brains) relative to WT littermates (black; 5 brains). (**E**) Fluorescence lifetime images of dendrites of WT and E5KO CA1 pyramidal neurons expressing Cdc42 FRET sensor before (0 min) and after (1 min) glutamate uncaging (HFU, yellow cross) on individual dendritic spines (yellow arrowheads). Warmer colors indicate sensor activation. (**F**) Target spines of E5KO (red) neurons show reduced HFU-induced Cdc42 activity relative to WT (black). (**G**) Peak Cdc42 activation (0 to 2 min post-HFU) is reduced in target spines of E5KO (red; 8 spines/8 cells) compared to WT (black; 9 spines/9 cells). (**H**) Fluorescence lifetime images of dendrites of WT and E5KO CA1 pyramidal neurons expressing RhoA FRET sensor before (0 min) and after (1 min) glutamate uncaging (HFU, yellow cross) on individual dendritic spines. (**I**) HFU-induced RhoA activity is robustly elevated in target spines of both WT (black) and E5KO (red) neurons. (**J**) Peak RhoA activation (0 to 2 min post-HFU) in target spines of E5KO (red; 8 spines/8 cells) is not different from those of WT (black; 9 spines/9 cells). Scale bars, 1 μm. Student's *t* test in (B), (D), (G) and (J). Data are presented as means ± SEM. $^{*}P < 0.05$ and $^{**}P < 0.01$. n.s., not significant.

Plasticity-associated activation of Cdc42, but not RhoA, is reduced in E5KO neurons

Given our finding that E5 regulates activation of both RhoA and Cdc42 in the brain, along with our prior results showing a role for E5 in facilitating activity-dependent new spine outgrowth (*19*), we hypothesized that during plasticity E5 substrate selectivity would be biased toward Cdc42, thus supporting spine growth and stabilization, rather than RhoA, which would support spine synapse shrinkage and elimination. To delineate E5 substrate selectivity downstream of neuronal activity that induces long-term plasticity in living neurons, we took advantage of well-characterized, genetically-encoded Rho GTPase FRET biosensors (*8*, *32*, *33*). These bimolecular sensors consist of an enhanced green fluorescent protein (eGFP)–tagged full-length GTPase that in the active, GTP-bound state binds the mCherry-tagged domain of a downstream effector protein (Rhotekin for RhoA and PAK for Cdc42), bringing the eGFP and mCherry fluorophores close enough to undergo FRET. Activation of the GTPase can, thus, be measured as a decrease in the lifetime of eGFP signal using fluorescence lifetime imaging microscopy (FLIM). Lifetime measurements were used to calculate the fraction of actively signaling molecules (Binding Fraction). In combination with two-photon glutamate uncaging to induce long-term plasticity at individual dendritic spines, these Rho GTPase FRET biosensors were used to measure activity-dependent Cdc42 or RhoA signaling in single spines.

To monitor the role of E5 in activity-dependent Cdc42 signaling, we transfected organotypic hippocampal slice cultures from E5KO and WT littermate mice with a bimolecular Cdc42 FRET sensor, consisting of eGFP-Cdc42 and mCherry-Pak3(60-113)-mCherry. Single spines on CA1 pyramidal neurons were stimulated using high-frequency glutamate uncaging (HFU) to induce long-term plasticity (*4*, *5*, *34*) while monitoring Cdc42 activation using time-lapse FLIM. Consistent with previous literature (*8*, *32*, *35*), HFU robustly activated Cdc42 within targeted spines (Fig. 1, E and F). Notably, we found that peak activation of Cdc42 (0 to 2 min following HFU) was reduced by ~50% in E5KO neurons compared to WT (Fig. 1G; E5KO, 0.04 ± 0.01; WT, 0.08 ± 0.01). This difference was independent of initial spine size, depth, or sensor expression differences (fig. S1, A to E). Furthermore, we found that the magnitude of spine growth was independent of initial Cdc42 activity but positively correlated with peak Cdc42 activity (fig. S1, F and G), consistent with a model in which Cdc42 activation promotes spine growth. Thus, we conclude that E5 is, in a large part, responsible for Cdc42 activation during the induction of long-term plasticity at individual synapses.

RhoA activation is also increased by plasticity-inducing synaptic activation (*8*, *32*). We therefore tested whether E5 also plays a role in activity-dependent RhoA activation. Hippocampal cultures from E5KO or WT littermate mice were transfected with a bimolecular RhoA FRET sensor, consisting of eGFP-RhoA and mCherry-Rhotekin(8-89)-mCherry, and individual spines were stimulated with HFU while RhoA activation was monitored using FLIM. Consistent with previous literature (*8*, *32*, *35*), we found that HFU robustly activated RhoA within targeted spines (Fig. 1, H and I). Intriguingly, HFU-induced RhoA activation was unaltered in E5KO spines relative to WT (Fig. 1J; E5KO, 0.06 ± 0.02; WT, 0.05 ± 0.01). As observed for Cdc42, no differences were detected in spine size, depth, or sensor expression between E5KO and WT (fig. S1, H to L). In contrast with Cdc42, the amount of spine growth was independent of both initial and peak RhoA activity (fig. S1, M and N), supporting a model in which spine growth is independent of the extent of activity-dependent RhoA activation. Because HFU-induced RhoA and Cdc42 activation are both downstream of the NMDA-type glutamate receptor (NMDAR) (*8*) but HFU-induced RhoA signaling remains intact in E5KO, we conclude that decreased HFU-induced Cdc42 activation in E5KO is not due to a disruption of NMDAR function in E5KO cells. Together, our results demonstrate that E5 contributes to activity-dependent Cdc42, but not RhoA, signaling in individual dendritic spines.

Ephexin5 tyrosine phosphorylation is developmentally regulated and activity dependent

Our data support that E5 selectively promotes Cdc42, but not RhoA, signaling during activity-dependent neuronal plasticity. Considering that E5 is widely recognized as a RhoA-GEF, we explored possible mechanisms that could explain how a RhoGEF could contribute to the differential activation of these two GTPase targets. Several RhoGEFs have been shown to undergo phosphorylation-dependent alterations in their activation or GTPase substrate selectivity (*28*, *29*, *36*–*38*). Because E5 tyrosine phosphorylation has been shown to be important for E5 signaling (*18*), we hypothesized that dynamic regulation of E5 tyrosine phosphorylation in the brain could control the selective activation of Cdc42 downstream of neuronal activity.

During the first two weeks of postnatal development, the mouse brain undergoes a large proliferation of dendritic spines, accompanied by increases in spontaneous neuronal activity (*39*). Therefore, we measured tyrosine-phosphorylated E5 (pTyr-E5) isolated from mouse brains at two points spanning an earlier and later part of this developmental time period. We used a custom-generated antibody (see Materials and Methods) to immunoprecipitate (IP) E5 from whole P7 or P19 mouse brains. We then measured E5 tyrosine phosphorylation using a pan-phosphotyrosine antibody (Fig. 2A). Notably, we found that the phosphotyrosine signal of the E5 IP relative to total E5 IP protein was markedly lower in P19 compared to P7 mice [Fig. 2B; E5-IP, pTyr/E5; P7, 1.05 ± 0.08; P19, 0.61 ± 0.07], despite the total E5 in the brain remaining unchanged (Fig. 2C; Input E5; P7, 0.91 ± 0.04; P19, 0.88 ± 0.09). Thus, the proportion of pTyr-E5 in the mouse brain decreases as synaptic connections are established across postnatal development.

We next asked whether a neuronal activation protocol that leads to long-term changes in synaptic strength could drive a reduction of relative pTyr-E5 levels, as observed across development. To test this, we induced neuronal activation in acute brain slices using chemical long-term potentiation (cLTP) and measured proportional pTyr-E5 levels from IP E5. We selected a cLTP protocol known to elicit long-term spine growth through an NMDAR-dependent mechanism (*40*). We treated acute slices from WT mice (P18 to P21) with forskolin (50 μM), rolipram (0.1 μM), and picrotoxin (100 μM) in 4 mM Ca^{2+}, 0 Mg^{2+} (cLTP), or with dimethyl sulfoxide (vehicle) for 5 or 20 min. Notably, we found that cLTP-treated samples had reduced pTyr-E5 levels compared to vehicle control [Fig. 2, D and E; E5-IP:pTyr/E5; vehicle (Veh.), 1.07 ± 0.10 (5 min) and 1.07 ± 0.28 (20 min); cLTP, 0.60 ± 0.16 (5 min) and 0.23 ± 0.04 (20 min)]. The total amount of E5 was not altered following cLTP treatment [Fig. 2, D and F; Input E5; Veh., 0.99 ± 0.17 (5 min) and 0.93 ± 0.19 (20 min); cLTP, 0.89 ± 0.16 (5 min) and 0.88 ± 0.18 (20 min)]. We confirmed the success of cLTP as, consistent with previous studies (*41*), cLTP induced strong phosphorylation of GluA1

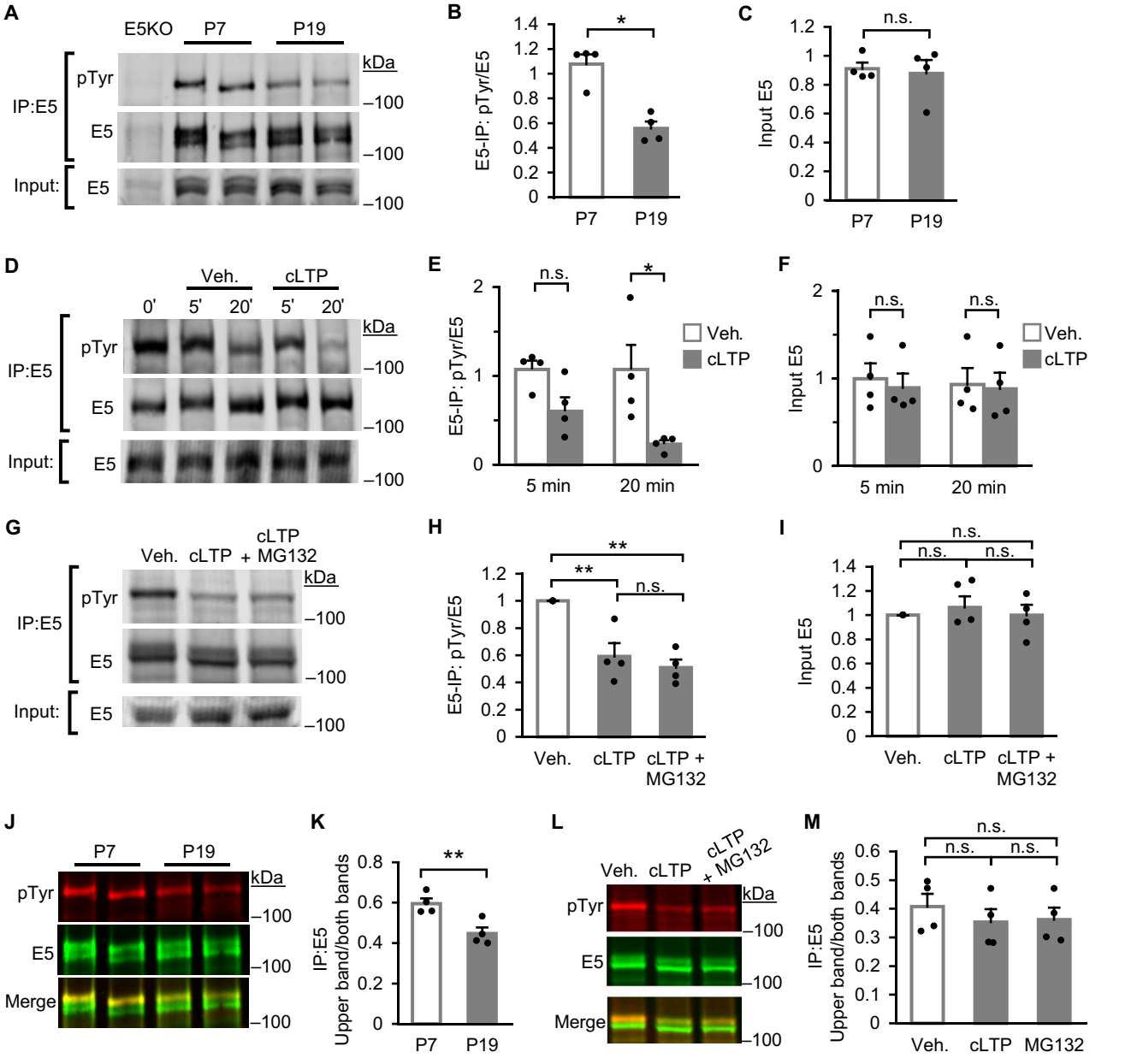

Fig. 2. E5 tyrosine phosphorylation is developmentally regulated and activity dependent. (**A**) Immunoblots of lysates from whole brains of P7 or P19 WT and E5KO mice subjected to IP by E5 antibody. (**B**) Pan-phosphotyrosine signal (pTyr)/E5 signal from IPed E5 (pTyr/E5) is lower in P19 (gray; 4 mice) compared to P7 (white; 4 mice) brains. (**C**) Input E5/total protein was not different between P7 (white; 4 mice) and P19 (gray; 4 mice). (**D**) Immunoblots of lysates from acute hippocampal slices treated with cLTP or vehicle for 5 or 20 min and subjected to IP by E5 antibody. (**E**) pTyr/E5 is reduced in cLTP (gray; 4 biological replicates) compared to vehicle (white; 4 biological replicates). (**F**) Input E5/total protein is unchanged in cLTP (gray; 4 replicates) compared to vehicle (white; 4 replicates). (**G**) Immunoblots of lysates from acute brain slices treated with cLTP, cLTP + MG132, or vehicle for 20 min and subjected to IP by E5 antibody. (**H**) pTyr/E5 is reduced in cLTP and cLTP + MG132 (gray; 4 biological replicates) compared to vehicle (white; 4 biological replicates). (**I**) Input E5/total protein is unchanged in cLTP and MG132 (gray; 4 biological replicates) compared to vehicle (white; 4 biological replicates). (**J**) Immunoblots from (A), highlighting the overlap of pTyr (red) and upper E5 (green) bands. (**K**) Proportion E5 in the upper band decreases from P7 to P19. (**L**) Immunoblots from (G), highlighting the overlap of pTyr (red) and E5 (green) bands. (**M**) Proportion of E5 in the upper band is unchanged following cLTP and cLTP + MG132. Two-way analysis of variance (ANOVA) with Bonferroni's correction for multiple comparisons in (E), (F), (H), (I), and (M) and Student's *t* test in (B), (C), and (K). Data are presented as means ± SEM. $^{*}P < 0.05$ and $^{**}P < 0.01$.

at S845 (fig. S2, A and B). Our results demonstrate that E5 tyrosine phosphorylation is reduced following LTP-inducing neuronal stimulation.

A decrease in relative pTyr-E5 levels could be due to the dephosphorylation of E5 or to the selective degradation of pTyr-E5, although the latter could be plausible if only a small proportion of E5 is pTyr-E5, as total E5 was unchanged across development and following cLTP (Fig. 2, C and F). To test whether selective protein degradation contributes to the cLTP-induced decrease in pTyr-E5, we repeated our cLTP experiments in the presence of the proteasome inhibitor MG132 or vehicle control. Notably, we found that MG132 did not affect the cLTP-induced decrease in pTyr-E5 levels relative to vehicle (Fig. 2, G and H; IP:E5 pTyr/E5; cLTP, 0.59 ± 0.09; cLTP + MG132, 0.51 ± 0.06), suggesting that reduced pTyr-E5 is not due to proteasomal-mediated degradation of pTyr-E5. Levels of total E5 were not altered (Fig. 2, G and I; Input E5; cLTP, 1.06 ± 0.09; cLTP + MG132, 1.00 ± 0.09). cLTP was successful (fig. S2, C and D) and MG132 was functional, as it increased protein ubiquitination, consistent with previous studies (*42*) (fig. S2E). Thus, our data support that the activity-dependent reduction of pTyr-E5 is not due to E5 degradation.

Indeed, a closer look at our data provided evidence supporting activity-dependent dephosphorylation of E5. We often observed E5 as multiple bands, consistent with published blots (*18*, *21*, *23*, *25*), and we noticed that the pTyr-E5 signal exclusively overlapped with the uppermost band (see Fig. 2J—data from Fig. 2A). During postnatal development, this upper E5 band was decreased relative to total E5 levels (Fig. 2, J and K; P7, 0.60 ± 0.03; P19, 0.45 ± 0.03), sufficient to account for around half of the previously observed decrease in pTyr signal (Fig. 2B). A similar analysis of data from our cLTP experiments showed that, again, pTyr-E5 signal exclusively overlapped with the uppermost band (see Fig. 2L—data from Fig. 2G). However, following cLTP, the upper E5 band did not decrease relative to total E5 levels (Fig. 2, L and M; Veh., 0.41 ± 0.04; cLTP, 0.35 ± 0.05; cLTP + MG132, 0.36 ± 0.04), indicating that the decrease in pTyr-E5 signal observed following cLTP represents a relatively small fraction of all E5. Together, our data support a model in which LTP-inducing neuronal activation at individual dendritic spines drives dephosphorylation, not degradation, of E5.

Ephexin5 Y361F mutation results in elevated Cdc42 activation in neurons

We next sought to determine how activity-dependent alterations in E5 tyrosine phosphorylation could affect E5-mediated GTPase activation. To address this question, we examined the consequences of blocking phosphorylation of E5 at residue Y361, a known E5 phosphorylation site that is part of a conserved regulatory motif in Ephexin family members (*29*, *30*, *43*). We measured Cdc42 and RhoA activity using GTPase FRET sensors in living neurons where endogenous E5 was replaced with the E5 containing the Y361F mutation ($E5^{Y361F}$), which is unable to be phosphorylated at Y361 (*18*).

We first assessed whether phosphorylation at E5 Y361 controls E5-dependent regulation of Cdc42 signaling. We expressed the Cdc42 FRET sensor in individual WT or E5KO neurons in organotypic hippocampal slices alongside either $E5^{WT}$, $E5^{Y361F}$, or GEF-dead E5 ($E5^{LQR}$) (*18*) and measured the activity of the Cdc42 FRET sensor using time-lapse FLIM. Notably, E5KO neurons expressing $E5^{Y361F}$ showed elevated Cdc42 activity compared to neurons expressing $E5^{WT}$ or $E5^{LQR}$ (Fig. 3, A and B; WT, 0.30 ± 0.04; $E5^{WT}$, 0.24 ± 0.03; $E5^{Y361F}$, 0.38 ± 0.03; $E5^{LQR}$, 0.21 ± 0.03), suggesting that

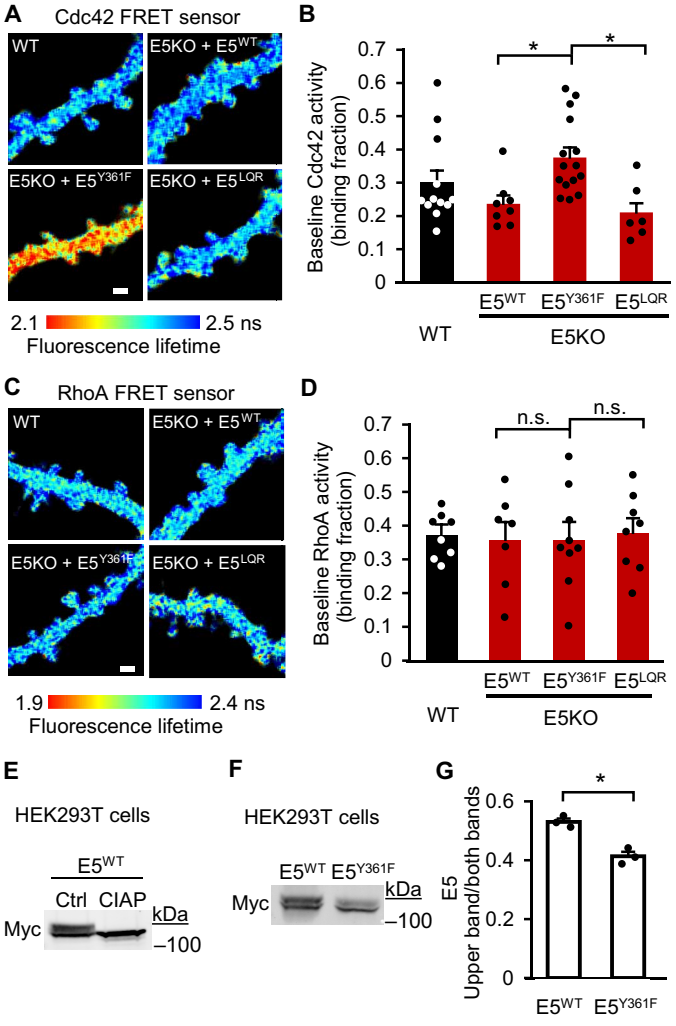

Fig. 3. Blocking phosphorylation of E5 at Y361 elevates Cdc42 activation. (**A**) Fluorescence lifetime images of dendrites of WT and E5KO CA1 pyramidal neurons expressing Cdc42 FRET biosensor and either $E5^{WT}$, $E5^{LQR}$, or $E5^{Y361F}$. Warmer colors indicate sensor activation. (**B**) Dendritic Cdc42 activation is elevated in E5KO neurons expressing $E5^{Y361F}$ (15 cells) compared to E5KO neurons expressing $E5^{WT}$ (8 cells) or $E5^{LQR}$ (6 cells). (**C**) Fluorescence lifetime images of dendrites of WT and E5KO CA1 pyramidal neurons expressing RhoA FRET biosensor and either $E5^{WT}$, $E5^{LQR}$, or $E5^{Y361F}$. (**D**) Dendritic RhoA activation is unchanged in E5KO neurons expressing $E5^{Y361F}$ (9 cells) compared to E5KO neurons expressing $E5^{WT}$ (7 cells) or $E5^{LQR}$ (8 cells). n.s., not significant. (**E**) Immunoblot of lysates from HEK293T cells expressing Myc-tagged $E5^{WT}$ treated with CIAP or vehicle control for 20 min. (**F**) Immunoblot of lysates from HEK293T cells expressing Myc-tagged $E5^{WT}$ or $E5^{Y361F}$. (**G**) Proportion of E5 in the upper band is lower for $E5^{Y361F}$ than for $E5^{WT}$. Scale bars, 1 μm. Two-way ANOVA with Bonferroni's correction for multiple comparisons in (B) and (D) and Student's *t* test in (G). Data are presented as means ± SEM. $^*P < 0.05$.

E5 phosphorylation at Y361 negatively regulates Cdc42 signaling. We confirmed the coexpression of all three E5 constructs alongside the Cdc42 FRET sensor using post hoc immunohistochemistry (IHC) (fig. S3, A and B) and the comparable expression of the Cdc42 FRET sensor between conditions by photon count (fig. S3C). Furthermore, we confirmed that all E5 constructs trafficked to spines at comparable levels using GFP-tagged E5 variants (fig. S3, D and E).

Thus, our results support that dephosphorylation of E5 at Y361 enhances Cdc42 signaling.

To assess whether phosphorylation at E5 Y361 also regulates E5-dependent regulation of RhoA, we used the same approach but, instead, with the RhoA FRET sensor. In contrast to results with Cdc42, we found that WT neurons and E5KO neurons expressing $E5^{WT}$, $E5^{Y361F}$, or $E5^{LQR}$ all exhibited similar RhoA activation levels (Fig. 3, C and D; WT, 0.37 ± 0.02; $E5^{WT}$, 0.36 ± 0.05; $E5^{Y361F}$, 0.36 ± 0.05; $E5^{LQR}$, 0.38 ± 0.04). Again, coexpression of E5 and sensor constructs was confirmed by post hoc IHC (fig. S3, F and G), and comparable expression of the RhoA FRET sensor between conditions was observed by photon count (fig. S3H). Thus, our combined results indicate that dephosphorylation of E5 at the Y361 residue selectively increases Cdc42, but not RhoA, activation.

Our data show that phosphomutation of a single E5 residue (Y361F) is sufficient to markedly enhance E5-mediated Cdc42 activation. Therefore, we wondered whether phosphorylation of this single Tyr residue would represent a major component of phosphorylated E5 under conditions that favored E5-mediated RhoA activation. Earlier studies highlighted the role of E5 in activating RhoA both in HEK293T cells and in early brain development (*18*, *21*). We therefore examined the consequences of the Y361F E5 phosphomutant on the proportion of phosphorylated E5 in HEK293 cells, as E5 mutants are only sparsely transfected in brain slices, making biochemistry not feasible. We expressed Myc-tagged $E5^{WT}$ and $E5^{Y361F}$ in HEK293T cells. First, we observed that, as in the brain, E5 protein ran as multiple bands (Fig. 3E) and that the upper band represented phosphorylated E5, as calf intestinal alkaline phosphatase (CIAP) treatment was sufficient to completely collapse the upper band into the bottom band (Fig. 3E). Notably, expression of Myc-tagged $E5^{Y361F}$ resulted in a ~22% decrease in the proportion of upper band E5 relative to total E5 (Fig. 3, F and G), demonstrating that the phosphorylation of E5 at Y361 represents a substantial proportion of phosphorylated E5 in HEK293 cells. Intriguingly, we observed a similar (~25%) decrease in the proportion of E5 in the upper band during brain development from P7 to P19 (Fig. 2H). Our data fit a model whereby, early in brain development, E5 is robustly phosphorylated at Y361 and predominately activates RhoA, whereas later in brain development, activity-dependent dephosphorylation at E5 Y361 drives the activation of Cdc42.

Ephexin5 GEF activity is required for activity-dependent long-term spine growth and Cdc42 signaling

Activity-dependent spine growth is vital for learning, both through the outgrowth of new spines supporting the formation of new circuit connections and through the growth of existing spines supporting the strengthening of existing connections (*1*, *4*). Our previous work indicated a role for E5 in facilitating activity-dependent outgrowth of nascent dendritic spines (*19*). We wondered whether E5 also contributes to the activity-dependent long-term growth of existing spines that accompanies synaptic strengthening.

To test the role of E5 in LTP-associated long-term spine growth, we implemented LTP-inducing HFU stimulation at individual spines of GFP-transfected E5KO and WT neurons and monitored subsequent changes in spine size. We stimulated single dendritic spines on CA1 pyramidal neurons in organotypic hippocampal slice cultures with HFU and then monitored their size using time-lapse two-photon imaging (Fig. 4, A and B). Notably, spines of E5KO neurons failed to undergo any sustained spine growth after HFU, in contrast with the robust long-term growth observed in the spines of WT littermates (Fig. 4C; E5KO, 97 ± 9%; WT, 211 ± 30%). These results were not explained by differences in initial spine size or depth between E5KO and WT neurons (fig. S4, A and B). Thus, our results support a requirement of E5 not only for activity-induced new spine outgrowth but also for the activity-dependent long-term spine growth associated with synaptic strengthening.

Loss of activity-dependent spine growth in E5KO neurons may be due to broader developmental consequences of genetic KO of E5 on synaptic function. Further, E5 could be required for long-term spine growth due to its enzymatic GEF activity or, alternatively, due to a structural function, such as scaffolding. Therefore, we examined whether the expression of E5 was sufficient to rescue the loss of HFU-induced spine growth in E5KO neurons using either full-length E5 ($E5^{WT}$) or a GEF-dead mutant of E5 ($E5^{LQR}$). We stimulated single dendritic spines on WT neurons expressing eGFP or on E5KO neurons coexpressing eGFP and either $E5^{WT}$ or $E5^{LQR}$ (Fig. 4, D and E). We found that spines on E5KO neurons expressing $E5^{WT}$ exhibited similar HFU-induced long-term growth as those on neurons from WT littermates (Fig. 4F; WT, 173 ± 21%; E5KO + $E5^{WT}$, 205 ± 26%). However, spines on E5KO neurons expressing $E5^{LQR}$ failed to undergo HFU-induced long-term spine growth (Fig. 4F; E5KO + $E5^{LQR}$, 101 ± 11%). No differences in initial spine size or depth between the different conditions were observed (fig. S4, C and D) and consistent expression of the E5 constructs in E5KO neurons was confirmed by IHC (fig. S4, E and F). Together, our data demonstrate that E5 GEF activity is required for the activity-dependent long-term growth of dendritic spines.

Next, we assessed whether the rescue of activity-dependent spine growth observed in $E5^{WT}$-expressing E5KO neurons was accompanied by a restoration of activity-dependent Cdc42 signaling. We expressed Cdc42 FRET sensor in WT or in E5KO neurons coexpressing either $E5^{WT}$ or $E5^{LQR}$ and measured Cdc42 activity during HFU at single dendritic spines (Fig. 4G). Notably, we observed that HFU-induced activation of Cdc42 in E5KO neurons expressing $E5^{LQR}$ was markedly reduced as compared to that observed in those expressing $E5^{WT}$ or as compared to WT neurons (Fig. 4, H and I; WT, 0.07 ± 0.01; $E5^{WT}$, 0.07 ± 0.01; E5KO + $E5^{LQR}$, 0.02 ± 0.01). Our results support that E5 GEF activity is required for the activity-dependent Cdc42 signaling that drives long-term spine growth.

Ephexin5 Y361F mutant rescues activity-dependent spine growth and Cdc42 signaling in E5KO neurons

Our finding that E5 is required for activity-dependent spine growth, that E5 contributes to the activation of Cdc42 during synaptic plasticity, and that the phosphomutant $E5^{Y361F}$ enhances baseline Cdc42 activation led us to hypothesize that the replacement of E5 with $E5^{Y361F}$ would be sufficient to rescue or enhance activity-dependent spine growth in E5KO neurons. To test our hypothesis, we stimulated single dendritic spines on E5KO neurons coexpressing eGFP and either $E5^{WT}$ or $E5^{Y361F}$ (Fig. 5, A and B). We found that the HFU-induced long-term spine growth on E5KO neurons expressing $E5^{Y361F}$ was not significantly different from neurons expressing $E5^{WT}$ (Fig. 5C; $E5^{WT}$, 159 ± 19%; $E5^{Y361F}$, 216 ± 35%; $P = 0.08$ by unpaired *t* test). There were no differences in initial spine size or depth between the different conditions (fig. S5, A and B). Thus, $E5^{Y361F}$ is sufficient to rescue plasticity-induced long-term spine growth in E5KO neurons.

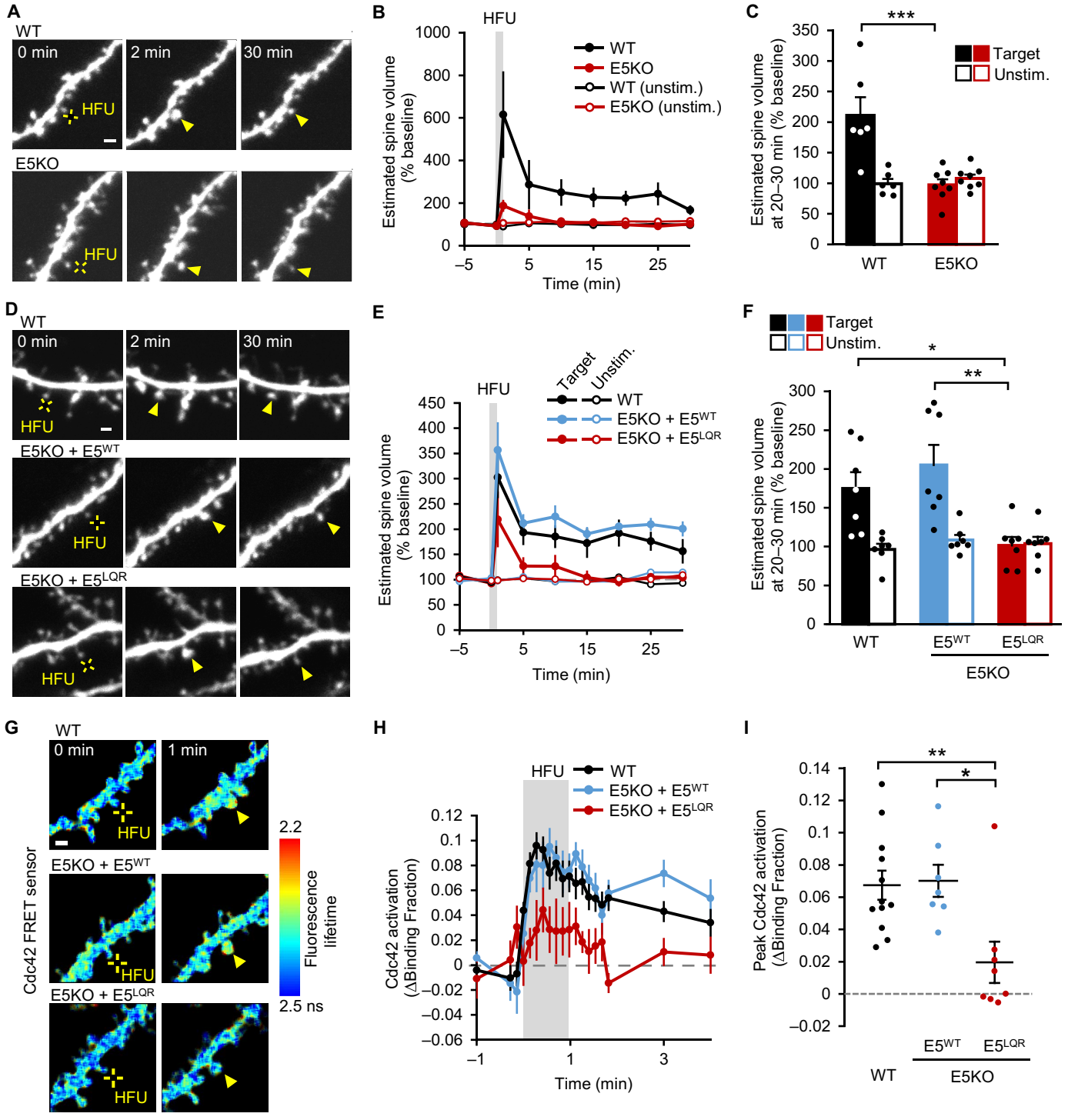

Fig. 4. E5 GEF activity is required for activity-dependent long-term spine growth and Cdc42 activation. (**A**) Images of dendrites from eGFP-expressing CA1 neurons in slice cultures from WT and E5KO animals before (0 min) and after (2 and 30 min) target spine (yellow arrowheads) stimulation with HFU (yellow cross). (**B** and **C**) Target spines from E5KO neurons (red; 8 spines/8 cells) did not show the HFU-induced long-term growth observed in spines from WT littermates (black; 6 spines/6 cells). Unstimulated (unstim.) spines (open circles) showed no changes. (**D**) Images of dendrites from WT CA1 neurons expressing eGFP (WT) or E5KO CA1 neurons coexpressing eGFP and $E5^{WT}$ or $E5^{LQR}$ before (0 min) and after (2 and 30 min) target spine (yellow arrowheads) stimulation with HFU (yellow cross). (**E** and **F**) Target spines from E5KO neurons expressing $E5^{LQR}$ (red; 7 spines/7 cells) did not show the HFU-induced long-term growth observed in E5KO neurons expressing $E5^{WT}$ (blue; 7 spines/7 cells) or WT control littermates (black; 7 spines/7 cells). Unstimulated spines (open circles) showed no changes. (**G**) Fluorescence lifetime images of dendrites from WT and E5KO neurons expressing Cdc42 FRET sensor and either $E5^{WT}$ or $E5^{LQR}$ before (0 min) and after (1 min) target spine (yellow arrowheads) stimulation with HFU (yellow cross). Warmer colors indicate sensor activation. (**H**) HFU-induced Cdc42 activation in target spines from WT neurons (black) or E5KO neurons expressing $E5^{WT}$ (blue) or $E5^{LQR}$ (red). (**I**) Peak Cdc42 activation (0 to 2 min post-HFU) is reduced in E5KO neurons expressing $E5^{LQR}$ (red; 8 spines/8 cells) compared to $E5^{WT}$ (blue; 7 spines/7 cells) and WT neurons (black; 12 spines/12 cells). Scale bars, 1 μm. Two-way ANOVA with Bonferroni's correction for multiple comparisons in (C) and (F) and Student's *t* test in (I). Data are presented as means ± SEM. $*P < 0.05$, $**P < 0.01$, and $***P < 0.001$.

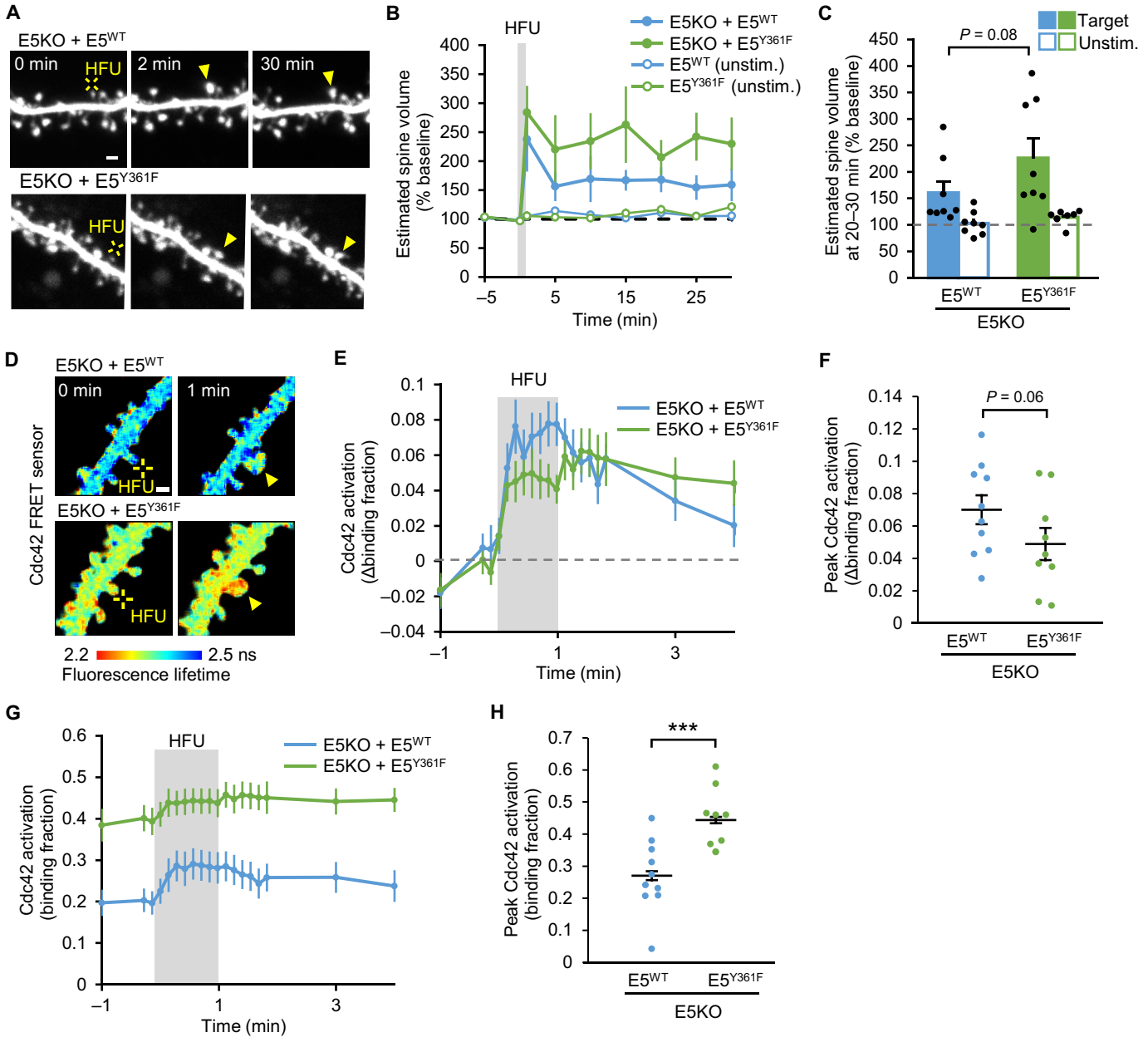

Fig. 5. E5 Y361F mutant rescues activity-dependent spine growth and Cdc42 activation in E5KO neurons. (**A**) Images of dendrites from E5KO CA1 neurons coexpressing eGFP and $E5^{WT}$ or $E5^{Y361F}$ before (0 min) and after (2 and 30 min) targetspine (yellow arrowheads) stimulation with HFU (yellow cross). (**B** and **C**) Target spines from E5KO neurons expressing $E5^{Y361F}$ (green; 9 spines/9 cells) showed a nonsignificant trend toward increased HFU-induced long-term growth as compared to $E5^{WT}$ (blue; 9 spines/9 cells). Unstimulated spines (open circles) showed no changes. (**D**) Fluorescence lifetime images of dendrites of E5KO neurons expressing Cdc42 FRET sensor and either $E5^{WT}$ or $E5^{Y361F}$ before (0 min) and after (1 min) target spine (yellow arrowheads) stimulation with HFU (yellow cross). Warmer colors indicate sensor activation. (**E**) HFU-induced Cdc42 activation in target spines from E5KO neurons expressing $E5^{WT}$ (blue) or $E5^{Y361F}$ (green). (**F**) E5KO neurons expressing $E5^{Y361F}$ (green; 9 spines/9 cells) showed a trend toward decreased peak Cdc42 activation (0 to 2 min post-HFU) compared to $E5^{WT}$ (blue; 10 spines/10 cells). (**G** and **H**) Baseline sensor activation, expressed as an unnormalized binding fraction, was markedly elevated in $E5^{Y361F}$ (green)–expressing cells compared to $E5^{WT}$ (blue)–expressing cells. Scale bars, 1 μm. Student's *t* test in (C), (F) and (H). Data are presented as means ± SEM. ***$P < 0.001$.

To assess the state of Cdc42 signaling during activity-dependent spine growth in $E5^{Y361F}$- versus $E5^{WT}$-expressing neurons, we stimulated single dendritic spines on E5KO neurons coexpressing Cdc42 FRET sensor and either $E5^{WT}$ or $E5^{Y361F}$ with HFU and measured the activity of Cdc42 using FLIM (Fig. 5, D and E). Given our results demonstrating an elevation in baseline Cdc42 activity in $E5^{Y361F}$-expressing neurons, we expected to observe at least a modestly increased Cdc42 signaling during the activity-dependent spine growth. Unexpectedly, we found that peak Cdc42 activation in $E5^{Y361F}$-expressing neurons was not significantly different from that in $E5^{WT}$-expressing neurons (Fig. 5F; $E5^{WT}$, 0.07 ± 0.01; $E5^{Y361F}$, 0.05 ± 0.01; $P = 0.06$ by unpaired *t* test). We wondered whether this unexpected

result might be due to a ceiling effect due to elevated baseline Cdc42 activity in $E5^{Y361F}$. Plotting the unnormalized baseline Cdc42 activity showed a marked elevation in $E5^{Y361F}$-expressing cells compared to those expressing $E5^{WT}$ (Fig. 5, G and H; $E5^{WT}$, 0.27 ± 0.04; $E5^{Y361F}$, 0.44 ± 0.03), consistent with our previous data. Together, we show that $E5^{Y361F}$ is sufficient to rescue activity-dependent spine growth and Cdc42 signaling in E5KO neurons, consistent with a model whereby the absence of E5 phosphorylation at Y361 supports activity-dependent spine growth.

DISCUSSION

Ephexin5 contributes to the activation of both Cdc42 and RhoA in neurons

Here, we show that E5 regulates both Cdc42 and RhoA activation in the brain. We further show that E5 promotes activity-dependent, postsynaptic Cdc42 signaling in neurons. Our results strongly support that Cdc42 is a substrate of neuronal E5, in contrast with earlier studies in the brain that highlight E5 as a RhoA-specific GEF (*18*, *20*, *21*). While surprising, we argue that these results are not unexpected, as nonneuronal studies have also identified E5 as an activator of multiple GTPases. Indeed, in pancreatic cancer–derived cell lines, knockdown of E5 reduces Cdc42, RhoA, and Rac1 activity, and overexpression leads to the activation of Cdc42, RhoA, and Rac1 (*26*). In vascular epithelial cells, E5 overexpression and knockdown lead to an increase and decrease in Cdc42 activation, respectively, and E5KO mice display retinal vascular defects consistent with loss of Cdc42 (*27*). We propose that neuronal E5 is capable of promoting both Cdc42 and RhoA activation under different physiological conditions.

Intriguingly, the ability to activate multiple GTPases may be a conserved feature among Ephexin family members. Ephexin1 overexpression leads to both RhoA and Cdc42 activation in cultured cortical neurons and the activation of Cdc42/Rac1 downstream effector Pak in HEK293T cells (*44*). In vitro nucleotide exchange assays have been used to demonstrate that Ephexin1 can activate both Cdc42 and RhoA (*29*, *30*). In addition to activating RhoA (*45*), Ephexin3 (Tim and Arhgef5) also activates Cdc42 in vitro (*46*), and Ephexin3 expression in COS-7 cells produces a phenotype consistent with Cdc42 activation (*47*). Notably, beyond the Ephexin family, for the larger group of around 70 Dbl family RhoGEFs, many are capable of activating multiple GTPases, including a handful that activate both Cdc42 and RhoA (*48*–*55*).

It remains an open question whether E5 activation of Cdc42 is the result of direct binding and nucleotide exchange or whether E5 leads to the activation of Cdc42 via an indirect means such as downstream cross-talk and mutual antagonism between RhoA and Cdc42 (*56*–*58*). Evidence for direct binding of multiple GTPases has been reported in the case of Ephexin1, which, when expressed without its N terminus, binds nucleotide-free RhoA and Cdc42 in activated GEF assays (*30*). In addition, in vitro nucleotide exchange assays, as discussed above, show that Ephexin1 and Ephexin3 activate both Cdc42 and RhoA (*29*, *30*, *44*, *46*). Because of the shared sequence similarity among Ephexins, particularly in their DH domains, which confer GTPase-binding specificity (*48*), it appears likely that E5 directly binds and activates Cdc42.

Ephexin5 substrate selectivity is regulated by neuronal activity and tyrosine phosphorylation

We found that E5 regulates both RhoA and Cdc42, two GTPases with markedly different roles in the regulation of the spine actin cytoskeleton: Activated RhoA promotes spine shrinkage and retraction, whereas activated Cdc42 drives spine growth and stabilization (*7*, *11*–*16*). How might a single RhoGEF coordinate the activation of opposing pathways? Earlier studies hint that the answer lies in spatiotemporal segregation of these processes by neuronal activity–dependent regulation. Although most studies reported E5 as an activator of RhoA that negatively regulates synapse density and spine outgrowth (*18*, *20*, *21*, *23*), E5, downstream of neuronal activity, instead acted to positively regulate spine outgrowth (*19*). Notably, neuronal activity has been shown to regulate both the activation (*59*, *60*) and synaptic localization (*61*, *62*) of other RhoGEFs. Our live-imaging data demonstrate that downstream of plasticity-inducing synaptic activation, E5 selectively plays a role in the activation of Cdc42, but not RhoA, signaling.

How does neuronal activity regulate E5? Neuronal activity has been shown in several studies to regulate the activation of RhoGEFs through phosphorylation (*21*, *28*, *59*, *60*, *63*, *64*). Indeed, we found that plasticity-inducing stimulation decreased the levels of tyrosine phosphorylation of E5. Furthermore, we showed that levels of pTyr-E5 are lowered in P19 mouse brains compared to P7, an age range across which there is an increase in activity-dependent refinement of neural circuits and the onset of critical periods for sensory modalities (*39*). The E5 single-point phosphomutant $E5^{Y361F}$ shows enhanced activation of Cdc42 and is sufficient to rescue plasticity-associated long-term spine growth. Together, we argue that neuronal activity regulates E5, at least in part, through the dynamic regulation of E5 tyrosine phosphorylation. Although we have provided evidence for one impactful phosphosite, it is likely that multiple phosphorylation states are integrated to confer E5 activation and GTPase selectivity.

How might neuronal activity result in reduced levels of tyrosine phosphorylated E5? One possibility is that neuronal activity induces rapid degradation of pTyr-E5. Tyrosine phosphorylated E5 has been shown to be targeted for ubiquitination and degradation (*18*). Furthermore, neuronal activity has been shown to lead to a rapid reduction in dendritic E5 signal that is dependent on proteasomal activity, while synaptic E5 was resistant to activity-dependent degradation (*19*). Alternatively, neuronal activity may induce rapid dephosphorylation of E5. We argue that, because the activity-dependent pTyr-E5 reduction was not blocked by the inhibition of the proteasome, our data support a mechanism of active dephosphorylation of E5 upon neuronal activity. Notably, several protein tyrosine phosphatases have been implicated in synaptic plasticity, such as STEP, PTP1B, and Shp2, which coordinate long-term depression (*65*), spine morphogenesis, (*66*), and LTP in hippocampal neurons (*67*, *68*). Further investigation into local interactors of E5 at the synapse may help resolve which phosphatases are implicated in the activity-dependent dephosphorylation of E5.

How does activity-dependent E5 tyrosine dephosphorylation drive Cdc42, but not RhoA, signaling? Our data support a model in which dephosphorylation of E5 at residue Y361 confers selective activation of Cdc42. Consistent with this model, we show that a large proportion of E5 expressed in HEK293T cells, from which E5 has been shown to robustly activate RhoA (*18*), is phosphorylated at Y361. Dephosphorylation of E5 Y361 could autonomously increase E5 activation of Cdc42 or, alternatively, it could alter the way E5 interfaces with intermediary proteins that facilitate E5 activation of Cdc42. E5 Y361 is part of a conserved regulatory motif on the N terminus, present in all Ephexins, dubbed the inhibitory helix, which interfaces with the DH domain (*30*, *43*). Notably, phosphorylation at the

homologous tyrosine has been reported to result in a shift in GTPase selectivity from Cdc42 and Rac1 to RhoA for Ephexin1 (*29*) and to lead to RhoA activation for Ephexin3 (*30*). Alternatively, mutation of Y361 could interfere with the regulation of E5, biasing it to bind and activate Cdc42. Ephexins are known to undergo intramolecular and intermolecular steric inhibition, which is sometimes regulated by the binding of other proteins (*43*, *69*, *70*). Mutation of the C-terminal SH3 domain of Ephexin1, which is thought to sterically block the GEF domain, increases Ephexin1 activation of Cdc42 (*30*). Thus, mutation of E5 Y361 may result in structural disruption that renders the GEF domain more accessible for Cdc42.

Ephexin5 regulates learning-associated neuronal plasticity

Regulation of Rho GTPases is crucial for the activity-dependent structural plasticity of dendritic spines that is thought to underlie learning and memory (*1*, *4*, *12*). Our earlier studies demonstrated a role for E5 in the regulation of synaptic plasticity, both in the baseline suppression of new spine outgrowth and in the activity-dependent promotion of new spine outgrowth that supports circuit rearrangements during learning (*19*). Here, we further demonstrate that E5 is vital for the activity-dependent long-term growth of existing spines that accompany synaptic strengthening during learning. We propose a model in which activity-dependent modulation of E5 tyrosine phosphorylation levels at synapses drives an alteration in the substrate selectivity of E5 from RhoA to Cdc42 and, thus, promotes the spine growth and stabilization vital for learning.

Our findings also provide insight into the role E5 plays in diseases that disrupt learning. E5 has been shown to be a key player in the spine loss seen in Alzheimer's disease. In postmortem human brain tissue, Alzheimer's model mice, and cells treated with amyloid-β, E5 levels are elevated, and it is thought that this increase in E5 leads to the activation of RhoA and, thus, spine elimination (*20*, *23*, *24*). However, recent studies examining the role of E5 in Angelman syndrome found that while levels of E5 in the brain are elevated, spine density is unexpectedly increased (*25*). Our results provide a possible mechanism for such an increase, as higher E5 levels could also support more activity-dependent spine stabilization, depending on the phosphorylation state and substrate selectivity of E5. This will be an important consideration in the development of E5 as a target for therapeutics (*24*).

MATERIALS AND METHODS

Animals

All experimental protocols were approved by the University of California, Davis Institutional Animal Care and Use Committee. Heterozygous E5KO mice in a C57BL/6J background were crossed to generate E5KO and WT littermate pairs.

Active GTPase pull-down assay

Whole mouse brains from P17 to P21 E5KO and WT littermate mice were lysed in ice-cold buffer containing 50 mM tris (pH 7.5), 150 mM NaCl, 5 mM $MgCl_2$, 5% glycerol, and 1% NP-40 alternative (MilliporeSigma) and centrifuged at 10,000*g* for 1 min to remove debris. Samples were incubated with either glutathione *S*-transferase (GST)–RBD or GST-PAK beads (Cytoskeleton Inc.) for 1 hour at 4°C, washed once in lysis buffer, boiled in Laemmli buffer, separated by SDS-PAGE, and transferred to a polyvinylidene difluoride (PVDF) membrane. Membranes were immunoblotted overnight with mouse anti-Cdc42 (Cytoskeleton Inc.; 1:250) or mouse anti-RhoA (Cytoskeleton Inc.; 1:500) and 1 hour with goat anti-mouse 680 (LI-COR; 1:15,000), directly before imaging on a LI-COR Odyssey Imaging system (LI-COR).

Preparation and transfection of organotypic hippocampal slice cultures

Organotypic hippocampal slices were prepared from P6 to P8 mice of both sexes, as previously described (*71*). Cultures were transfected 1 day before imaging with biolistic gene transfer, as previously described (*72*). DNA was coated onto 6 to 8 mg of 1.6-μm gold beads. For experiments using GTPase FRET sensors, either 15 μg each of eGFP-Cdc42 and mCherry-Pak3(60-113)-mCherry or eGFP-RhoA and mCherry-Rhotekin(8-89)-mCherry (Addgene) were used. For experiments coexpressing E5 constructs, 25 μg of $E5^{WT}$, $E5Y^{361F}$, or $E5^{LQR}$ was used. For experiments expressing eGFP, 10 μg of eGFP (Clontech) was used. For experiments expressing GFP-tagged E5 constructs, 10 μg of $E5^{WT}$-GFP, $E5^{LQR}$-GFP, and $E5^{Y361F}$-GFP, along with 20 μg of DsRed-Express2, were used.

Time-lapse two-photon imaging of spine structural plasticity

Transfected CA1 pyramidal neurons (10 to 14 days in vitro) at depths of 10 to 50 μm were imaged using a custom two-photon microscope (*73*) with a Ti:sapphire laser (930 nm; Spectra-Physics, Mai Tai) controlled with ScanImage (*74*). Image stacks with 1-μm *z*-steps (512 pixels by 512 pixels, 0.02 μm per pixel) were collected. For each neuron, one segment of secondary or tertiary basal dendrite was imaged for 30 min at 29° to 30°C in recirculating artificial cerebral spinal fluid [ACSF; 127 mM NaCl, 25 mM $NaHCO_3$, 1.2 mM NaH_2PO_4, 2.5 mM KCl, 25 mM D-glucose, aerated with 95% O_2/5% CO_2, and ~310 mOsm (pH 7.2)] with 1 μM tetrodotoxin (TTX), 0 mM Mg^{2+}, 2 mM Ca^{2+}, and 2.5 mM MNI-glutamate (Tocris).

Fluorescence lifetime imaging microscopy

Fluorescence lifetime was measured using time-correlated photon counting (Becker & Hickl Gmbh), as previously described (*8*, *75*). The microscope setup and experimental conditions were as described above, except that FLIM data were obtained using a GaAs(P) photosensor (H7422PA-40, Hamamatsu) and a time-correlated single photon counting board (SPC-150, Becker and Hickl) controlled with custom software (*75*). In addition, in the case of FLIM, single-plane images (128 pixels by 128 pixels, 0.07 μm per pixel) were collected.

Photolysis of MNI-caged glutamate with HFU stimulation

HFU consisted of either 30 pulses (720 nm, 6-ms duration, and ~4 to 5 mW at the sample) at 0.5 Hz for FLIM or 60 pulses (720 nm, 2-ms duration, and ~7 to 8 mW at the sample) at 2 Hz for spine structural plasticity. The beam was parked at a point ~0.5 to 1 μm from the spine at the position farthest from the dendrite. Healthy and stimulus responsive cells were selected on the basis of a test HFU stimulus at a test spine on a different dendrite than the target spine. Spines targeted for HFU stimulation were well isolated and of an average size that did not fluctuate during baseline imaging.

Preparation of acute brain slices and chemical LTP treatment

Acute brain slices were prepared, as previously described (*76*), from P17 to P21 C57BL/6N mice of both sexes. Coronal 300-μm

slices were cut (Leica VT100S vibratome) in cold choline chloride dissection solution containing 110 mM choline chloride, 2.5 mM KCl, 25 mM $NaHCO_3$, 0.5 mM $CaCl_2$, 7 mM $MgCl_2$, 1.3 mM NaH_2PO_4, 11.6 mM sodium ascorbate, 3.1 mM sodium pyruvate, and 25 mM glucose, saturated with 95% O_2/5% CO_2. Slices were recovered first at 32°C for 30 min in an oxygenated ACSF before cLTP treatment. cLTP was performed by transferring slices to oxygenated ACSF containing either 50 μM forskolin, 0.1 μM rolipram, 0.1 μM picrotoxin (PTX), 4 mM $CaCl_2$, and 0 $MgCl_2$ or equal volume dimethyl sulfoxide with 2 mM $CaCl_2$ and 1 mM $MgCl_2$ for 5 to 20 min at 32°C before removing slices from the liquid and lysing in radioimmunoprecipitation assay buffer. For experiments with MG132, slices were preincubated in ACSF containing 10 μM MG132 at 32°C for 20 min before transfer to ACSF containing cLTP reagents and 10 μM MG132 for 20 min.

Custom E5 antibody generation and E5 IP

Polyclonal antibodies specific to E5 were generated by injecting rabbits with the following peptide sequences: E5 13 to 25 (PTLKPPRIIRPRPPSRHC) and E5 277 to 288 (RKLPPLKPPKPTKVRQDC) labeled E5-NT and E5-MID, respectively. Serum from injected rabbits was subjected to affinity purification with KLH–conjugated peptides. Resulting polyclonal antibodies were validated using brain tissue from E5KO mice. E5-NT was used in all figures to identify E5 via immunoblot. IP of E5 was performed by incubating E5-MID antibody with Protein G Dynabeads (Invitrogen) for 30 min at room temperature, followed by washing three times with tris-buffered saline (TBS) with 0.02% Tween 20 before incubating the beads with a tissue sample (lysed in radioimmunoprecipitation assay buffer) for 1 hour at 4°C, washing three times with tris-buffered saline with 0.02% Tween 20, and boiling in Laemmli buffer, then separation by SDS-PAGE, and transfer to PVDF membrane. Membranes were subjected to total protein staining (Revert 700, LI-COR) following the manufacturer's recommendations, then immunoblotted overnight with primary antibody: rabbit anti–E5-NT (1:100); mouse anti-phosphotyrosine (Sigma-Aldrich; 1:500); anti-GluA1 (1:1000) (*77*, *78*); rabbit anti-GluA1 phospho-S845 (Abcam; 1:1000); mouse anti-ubiquitin (Enzo; 1:500); mouse anti-polyubiquitinylated conjugates (Enzo; 1:500); anti-Myc (Invitrogen; 1:500); and 1 hour with secondary antibody (goat anti-mouse 680, LI-COR; 1:15,000; goat antirabbit 800, LI-COR; 1:15,000) before imaging.

Culturing and transfection of HEK293T cells

HEK293T cell cultures were maintained in Dulbecco's modified Eagle's medium (DMEM; Gibco) and supplemented with 10% fetal bovine serum (Gibco) and penicillin-streptomycin (Gibco). Transfection was conducted with Lipofectamine 2000 (Invitrogen) using the manufacturer's recommended protocol 24 hours before harvesting.

Alkaline phosphatase treatment

Whole P17 mouse brains were lysed in ice-cold buffer containing 100 mM NaCl, 50 mM tris, 10 mM $MgCl_2$, and 1% NP-40 alternative (MilliporeSigma) and centrifuged at 10,000*g* for 1 min to remove debris. Samples were treated with 1 U of CIAP (MilliporeSigma) per 2 μg of protein for 20 min at 37°C, then immediately boiled in Laemmli buffer, separated by SDS-PAGE, and transferred to a PVDF membrane.

Immunohistochemistry

Organotypic slices were fixed in 4% paraformaldehyde for 1 hour at 4°C, washed three times with phosphate-buffered saline (PBS), and blocked in 5% goat serum in PBS with 0.03% Triton X-100 for 2 hours before incubation with mouse anti-Myc 9e10 (Invitrogen; 1:1000) overnight at 4°C. Slices were then washed three times with PBS with 0.03% Triton X-100 and incubated with secondary antibodies (goat anti-mouse immunoglobulin G Alexa Fluor 350 when coexpressed with FRET sensor or goat anti-mouse immunoglobulin G Alexa Fluor 555; Thermo Fisher Scientific) for 4 hours at room temperature, followed by washing three times with PBS with 0.03% Triton X-100. Slices were mounted in ProLong Gold (Life Technologies).

Statistical analysis

Quantification of data from live-cell imaging experiments

For FLIM experiments, differences in measured lifetime from the empirically known lifetime of eGFP were used to calculate the fraction of actively signaling molecules, referred to as the binding fraction (*75*). Using lifetime measurements, the average binding fraction of the sensor was calculated from regions of interest (ROIs) encompassing the target dendritic spine or from ROIs on the dendrite. For two-photon time-lapse imaging of spine structural plasticity, the background-subtracted integrated green fluorescence signal in ROIs, encasing the entire spine of interest or neighbor spines, was used to estimate spine volume. All isolated spines within the ROI were analyzed as unstimulated neighbors. Spine enrichment analysis was performed as previously described (*73*); briefly, background-subtracted green fluorescence intensity (from eGFP-tagged constructs) of spines/dendrites was divided by the background-subtracted red fluorescence intensity (from DsRed-Express2 cell fill) of spines/dendrites.

Quantification of data from Western blot experiments

Images from the LI-COR Odyssey Imaging system were quantified using Fiji. For total protein stain, integrated pixel density from whole lanes was background subtracted using background values to the left and right of the lane. For bands from proteins of interest, the integrated pixel density of bands of interest was background subtracted using background values within the lane of interest above and below the band. Band intensity was normalized only to values obtained from the same blot.

Quantification of IHC

Immunostained neurons were imaged on a Zeiss Apotome 3 microscope with excitation light power and exposure times held constant. Whole-cell images were acquired as 1-μm Z-stacks. Quantification of Myc-tagged E5 WT and E5 mutant protein expression levels was performed in Fiji by measuring background-subtracted fluorescence intensity from a 30-μm–diameter ROI, encompassing the soma of each cell, taken from single plane images within the Z-stack at the center of the soma.

Statistical tests and sample sizes

Statistical tests were performed using GraphPad Prism Software. For all live-imaging experiments, *n* values represent individual neurons, and each experimental condition includes hippocampal slices from at least four individual animals. For acute slice biochemistry, two technical replicates were averaged together to generate a single *n* value that represents a biological replicate, and each experimental condition includes, at minimum, four individual animals. Test types, sample sizes, and significance are described in figure legends. Data in text are presented as mean ± SEM.

Supplementary Materials

This PDF file includes:

Figs. S1 to S5

REFERENCES AND NOTES

1. A. Hayashi-Takagi, S. Yagishita, M. Nakamura, F. Shirai, Y. Wu, A. L. Loshbaugh, B. Kuhlman, K. M. Hahn, H. Kasai, Labelling and optical erasure of synaptic memory traces in the motor cortex. *Nature* **525**, 333–338 (2015).
2. A. Holtmaat, L. Wilbrecht, G. W. Knott, E. Welker, K. Svoboda, Experience-dependent and cell-type-specific spine growth in the neocortex. *Nature* **441**, 979–983 (2006).
3. H. Kasai, N. E. Ziv, H. Okazaki, S. Yagishita, T. Toyoizumi, Spine dynamics in the brain, mental disorders and artificial neural networks. *Nat. Rev. Neurosci.* **22**, 407–422 (2021).
4. M. Matsuzaki, N. Honkura, G. C. R. Ellis-Davies, H. Kasai, Structural basis of long-term potentiation in single dendritic spines. *Nature* **429**, 761–766 (2004).
5. M. Bosch, J. Castro, T. Saneyoshi, H. Matsuno, M. Sur, Y. Hayashi, Structural and molecular remodeling of dendritic spine substructures during long-term potentiation. *Neuron* **82**, 444–459 (2014).
6. J. G. Duman, F. A. Blanco, C. A. Cronkite, Q. Ru, K. C. Erikson, S. Mulherkar, A. B. Saifullah, K. Firozi, K. F. Tolias, Rac-maninoff and Rho-vel: The symphony of Rho-GTPase signaling at excitatory synapses. *Small GTPases* **13**, 14–47 (2022).
7. I. H. Kim, H. Wang, S. H. Soderling, R. Yasuda, Loss of Cdc42 leads to defects in synaptic plasticity and remote memory recall. *eLife* **3**, e02839 (2014).
8. H. Murakoshi, H. Wang, R. Yasuda, Local, persistent activation of Rho GTPases during plasticity of single dendritic spines. *Nature* **472**, 100–104 (2011).
9. Y. Nakahata, R. Yasuda, Plasticity of spine structure: Local signaling, translation and cytoskeletal reorganization. *Front. Synaptic Neurosci.* **10**, 29 (2018).
10. K.-I. Okamoto, T. Nagai, A. Miyawaki, Y. Hayashi, Rapid and persistent modulation of actin dynamics regulates postsynaptic reorganization underlying bidirectional plasticity. *Nat. Neurosci.* **7**, 1104–1112 (2004).
11. S. E. Newey, V. Velamoor, E.-E. Govek, L. Van Aelst, Rho GTPases, dendritic structure, and mental retardation. *J. Neurobiol.* **64**, 58–74 (2005).
12. K. F. Tolias, J. G. Duman, K. Um, Control of synapse development and plasticity by Rho GTPase regulatory proteins. *Prog. Neurobiol.* **94**, 133–148 (2011).
13. A. Tashiro, A. Minden, R. Yuste, Regulation of dendritic spine morphology by the Rho family of small GTPases: Antagonistic roles of Rac and Rho. *Cereb. Cortex* **10**, 927–938 (2000).
14. A. Y. Nakayama, M. B. Harms, L. Luo, Small GTPases Rac and Rho in the maintenance of dendritic spines and branches in hippocampal pyramidal neurons. *J. Neurosci.* **20**, 5329–5338 (2000).
15. F. Irie, Y. Yamaguchi, EphB receptors regulate dendritic spine development via intersectin, Cdc42 and N-WASP. *Nat. Neurosci.* **5**, 1117–1118 (2002).
16. A. Tashiro, R. Yuste, Regulation of dendritic spine motility and stability by Rac1 and Rho kinase: Evidence for two forms of spine motility. *Mol. Cell. Neurosci.* **26**, 429–440 (2004).
17. A. Schmidt, A. Hall, Guanine nucleotide exchange factors for Rho GTPases: Turning on the switch. *Genes Dev.* **16**, 1587–1609 (2002).
18. S. S. Margolis, J. Salogiannis, D. M. Lipton, C. Mandel-Brehm, Z. P. Wills, A. R. Mardinly, L. Hu, P. L. Greer, J. B. Bikoff, H.-Y. H. Ho, M. J. Soskis, M. Sahin, M. E. Greenberg, EphB-mediated degradation of the RhoA GEF Ephexin5 relieves a developmental brake on excitatory synapse formation. *Cell* **143**, 442–455 (2010).
19. A. Hamilton, J. Lambert, L. Parajuli, O. Vivas, D. Park, I. Stein, J. Jahncke, M. Greenberg, S. Margolis, K. Zito, A dual role for the RhoGEF Ephexin5 in regulation of dendritic spine outgrowth. *Mol. Cell. Neurosci.* **80**, 66–74 (2017).
20. M. Olabarria, S. Pasini, C. Corona, P. Robador, C. Song, H. Patel, R. Lefort, Dysfunction of the ubiquitin ligase E3A Ube3A/E6-AP contributes to synaptic pathology in Alzheimer's disease. *Commun. Biol.* **2**, 111 (2019).
21. T. B. Schaffer, J. E. Smith, E. K. Cook, T. Phan, S. S. Margolis, PKCε inhibits neuronal dendritic spine development through dual phosphorylation of Ephexin5. *Cell Rep.* **25**, 2470–2483.e8 (2018).
22. H. Ogita, S. Kunimoto, Y. Kamioka, H. Sawa, M. Masuda, N. Mochizuki, EphA4-mediated Rho activation via Vsm-RhoGEF expressed specifically in vascular smooth muscle cells. *Circ. Res.* **93**, 23–31 (2003).
23. G. L. Sell, T. B. Schaffer, S. S. Margolis, Reducing expression of synapse-restricting protein Ephexin5 ameliorates Alzheimer's-like impairment in mice. *J. Clin. Invest.* **127**, 1646–1650 (2017).
24. E. K. Cook, G. L. Sell, T. B. Schaffer, S. S. Margolis, The emergence of Ephexin5 as a therapeutic target in Alzheimer's disease. *Expert Opin. Ther. Targets* **23**, 263–265 (2019).
25. G. L. Sell, W. Xin, E. K. Cook, M. A. Zbinden, T. B. Schaffer, R. N. O'Meally, R. N. Cole, S. S. Margolis, Deleting a UBE3A substrate rescues impaired hippocampal physiology and learning in Angelman syndrome mice. *Sci. Rep.* **11**, 19414 (2021).
26. H. Fukushima, M. Yasumoto, S. Ogasawara, J. Akiba, Y. Kitasato, M. Nakayama, Y. Naito, Y. Ishida, Y. Okabe, M. Yasunaga, H. Horiuchi, E. Sakamoto, H. Itadani, S. Mizuarai, S. Oie, H. Yano, ARHGEF15 overexpression worsens the prognosis in patients with pancreatic ductal adenocarcinoma through enhancing the motility and proliferative activity of the cancer cells. *Mol. Cancer* **15**, 32 (2016).
27. S. Kusuhara, Y. Fukushima, S. Fukuhara, L. M. Jakt, M. Okada, Y. Shimizu, M. Hata, K. Nishida, A. Negi, M. Hirashima, N. Mochizuki, S.-I. Nishikawa, A. Uemura, Arhgef15 promotes retinal angiogenesis by mediating VEGF-induced Cdc42 activation and potentiating RhoJ inactivation in endothelial cells. *PLOS ONE* **7**, e45858 (2012).
28. M. Patel, A. V. Karginov, Phosphorylation-mediated regulation of GEFs for RhoA. *Cell Adh. Migr.* **8**, 11–18 (2014).
29. M. Sahin, P. L. Greer, M. Z. Lin, H. Poucher, J. Eberhart, S. Schmidt, T. M. Wright, S. M. Shamah, S. O'Connell, C. W. Cowan, L. Hu, J. L. Goldberg, A. Debant, G. Corfas, C. E. Krull, M. E. Greenberg, Eph-dependent tyrosine phosphorylation of ephexin1 modulates growth cone collapse. *Neuron* **46**, 191–204 (2005).
30. M. E. Yohe, K. Rossman, J. Sondek, Role of the C-terminal SH3 domain and N-terminal tyrosine phosphorylation in regulation of Tim and related Dbl-family proteins. *Biochemistry* **47**, 6827–6839 (2008).
31. M. J. Baker, I. Rubio, Active GTPase pulldown protocol, in *Ras Activity and Signaling: Methods and Protocols*, I. Rubio, I. Prior, Eds., *Methods in Molecular Biology* (Springer, 2021), pp. 117–135.
32. N. G. Hedrick, S. C. Harward, C. E. Hall, H. Murakoshi, J. O. McNamara, R. Yasuda, Rho GTPase complementation underlies BDNF-dependent homo- and heterosynaptic plasticity. *Nature* **538**, 104–108 (2016).
33. T. Saneyoshi, H. Matsuno, A. Suzuki, H. Murakoshi, N. G. Hedrick, E. Agnello, R. O'Connell, M. M. Stratton, R. Yasuda, Y. Hayashi, Reciprocal activation within a kinase-effector complex underlying persistence of structural LTP. *Neuron* **102**, 1199–1210.e6 (2019).
34. I. S. Stein, T. C. Hill, W. C. Oh, L. K. Parajuli, K. Zito, Two-photon glutamate uncaging to study structural and functional plasticity of dendritic spines, in *Multiphoton Microscopy*, vol. 148 of *Neuromethods*, E. Hartveit, Ed. (Springer, 2019), pp. 65–85.
35. A. C. E. Shibata, H. H. Ueda, K. Eto, M. Onda, A. Sato, T. Ohba, J. Nabekura, H. Murakoshi, Photoactivatable CaMKII induces synaptic plasticity in single synapses. *Nat. Commun.* **12**, 751 (2021).
36. C. W. Cowan, Y. R. Shao, M. Sahin, S. M. Shamah, M. Z. Lin, P. L. Greer, S. Gao, E. C. Griffith, J. S. Brugge, M. E. Greenberg, Vav family GEFs link activated Ephs to endocytosis and axon guidance. *Neuron* **46**, 205–217 (2005).
37. M. Gupta, X. Qi, V. Thakur, D. Manor, Tyrosine phosphorylation of Dbl regulates GTPase signaling. *J. Biol. Chem.* **289**, 17195–17202 (2014).
38. G. Lazer, L. Pe'er, M. Farago, K. Machida, B. J. Mayer, S. Katzav, Tyrosine residues at the carboxyl terminus of Vav1 play an important role in regulation of its biological activity. *J. Biol. Chem.* **285**, 23075–23085 (2010).
39. C. Lohmann, H. W. Kessels, The developmental stages of synaptic plasticity. *J. Physiol.* **592**, 13–31 (2014).
40. C. D. Kopec, B. Li, W. Wei, J. Boehm, R. Malinow, Glutamate receptor exocytosis and spine enlargement during chemically induced long-term potentiation. *J. Neurosci.* **26**, 2000–2009 (2006).
41. Y. Lu, M. Allen, A. R. Halt, M. Weisenhaus, R. F. Dallapiazza, D. D. Hall, Y. M. Usachev, G. S. McKnight, J. W. Hell, Age-dependent requirement of AKAP150-anchored PKA and GluR2-lacking AMPA receptors in LTP. *EMBO J.* **26**, 4879–4890 (2007).
42. G. N. Patrick, B. Bingol, H. A. Weld, E. M. Schuman, Ubiquitin-mediated proteasome activity is required for agonist-induced endocytosis of GluRs. *Curr. Biol.* **13**, 2073–2081 (2003).
43. M. Zhang, L. Lin, C. Wang, J. Zhu, Double inhibition and activation mechanisms of Ephexin family RhoGEFs. *Proc. Natl. Acad. Sci. U.S.A.* **118**, e2024465118 (2021).
44. S. M. Shamah, M. Z. Lin, J. L. Goldberg, S. Estrach, M. Sahin, L. Hu, M. Bazalakova, R. L. Neve, G. Corfas, A. Debant, M. E. Greenberg, EphA receptors regulate growth cone dynamics through the novel guanine nucleotide exchange factor ephexin. *Cell* **105**, 233–244 (2001).
45. M. E. Yohe, K. L. Rossman, O. S. Gardner, A. E. Karnoub, J. T. Snyder, S. Gershburg, L. M. Graves, C. J. Der, J. Sondek, Auto-inhibition of the Dbl family protein Tim by an N-terminal helical motif. *J. Biol. Chem.* **282**, 13813–13823 (2007).
46. X. Xie, S. W. Chang, T. Tatsumoto, A. M. L. Chan, T. Miki, TIM, a Dbl-related protein, regulates cell shape and cytoskeletal organization in a Rho-dependent manner. *Cell. Signal.* **17**, 461–471 (2005).
47. M.-A. Debily, A. Camarca, M. Ciullo, C. Mayer, S. El Marhomy, I. Ba, A. Jalil, A. Anzisi, J. Guardiola, D. Piatier-Tonneau, Expression and molecular characterization of alternative transcripts of the ARHGEF5/TIM oncogene specific for human breast cancer. *Hum. Mol. Genet.* **13**, 323–334 (2004).
48. K. L. Rossman, C. J. Der, J. Sondek, GEF means go: Turning on RHO GTPases with guanine nucleotide-exchange factors. *Nat. Rev. Mol. Cell Biol.* **6**, 167–180 (2005).
49. K. Abe, K. L. Rossman, B. Liu, K. D. Ritola, D. Chiang, S. L. Campbell, K. Burridge, C. J. Der, Vav2 is an activator of Cdc42, Rac1, and RhoA. *J. Biol. Chem.* **275**, 10141–10149 (2000).

50. B. P. Liu, K. Burridge, Vav2 activates Rac1, Cdc42, and RhoA downstream from growth factor receptors but not β1 integrins. *Mol. Cell. Biol.* **20**, 7160–7169 (2000).
51. T. Tatsumoto, X. Xie, R. Blumenthal, I. Okamoto, T. Miki, Human Ect2 is an exchange factor for Rho Gtpases, phosphorylated in G2/M phases, and involved in cytokinesis. *J. Cell Biol.* **147**, 921–928 (1999).
52. P. A. Solski, R. S. Wilder, K. L. Rossman, J. Sondek, A. D. Cox, S. L. Campbell, C. J. Der, Requirement for C-terminal sequences in regulation of Ect2 guanine nucleotide exchange specificity and transformation. *J. Biol. Chem.* **279**, 25226–25233 (2004).
53. M. J. Hart, A. Eva, T. Evans, S. A. Aaronson, R. A. Cerione, Catalysis of guanine nucleotide exchange on the CDC42Hs protein by the *dbl* oncogene product. *Nature* **354**, 311–314 (1991).
54. M. J. Hart, A. Eva, D. Zangrilli, S. A. Aaronson, T. Evans, R. A. Cerione, Y. Zheng, Cellular transformation and guanine nucleotide exchange activity are catalyzed by a common domain on the dbl oncogene product. *J. Biol. Chem.* **269**, 62–65 (1994).
55. K. Komai, R. Okayama, M. Kitagawa, H. Yagi, K. Chihara, S. Shiozawa, Alternative splicing variants of the human *DBL* (*MCF-2*) proto-oncogene. *Biochem. Biophys. Res. Commun.* **299**, 455–458 (2002).
56. H. W. Yang, S. R. Collins, T. Meyer, Locally excitable Cdc42 signals steer cells during chemotaxis. *Nat. Cell Biol.* **18**, 191–201 (2016).
57. J. G. Duman, S. Mulherkar, Y.-K. Tu, J. Cheng, K. F. Tolias, Mechanisms for spatiotemporal regulation of Rho-GTPase signaling at synapses. *Neurosci. Lett.* **601**, 4–10 (2015).
58. C. Zmurchok, W. R. Holmes, Simple Rho GTPase dynamics generate a complex regulatory landscape associated with cell shape. *Biophys. J.* **118**, 1438–1454 (2020).
59. K. F. Tolias, J. B. Bikoff, A. Burette, S. Paradis, D. Harrar, S. Tavazoie, R. J. Weinberg, M. E. Greenberg, The Rac1-GEF Tiam1 couples the NMDA receptor to the activity-dependent development of dendritic arbors and spines. *Neuron* **45**, 525–538 (2005).
60. Z. Xie, D. P. Srivastava, H. Photowala, L. Kai, M. E. Cahill, K. M. Woolfrey, C. Y. Shum, D. J. Surmeier, P. Penzes, Kalirin-7 controls activity-dependent structural and functional plasticity of dendritic spines. *Neuron* **56**, 640–656 (2007).
61. E. C. Muly, A. C. Nairn, P. Greengard, D. G. Rainnie, Subcellular distribution of the Rho-GEF Lfc in primate prefrontal cortex: Effect of neuronal activation. *J. Comp. Neurol.* **508**, 927–939 (2008).
62. X. P. Ryan, J. Alldritt, P. Svenningsson, P. B. Allen, G.-Y. Wu, A. C. Nairn, P. Greengard, The Rho-specific GEF Lfc interacts with neurabin and spinophilin to regulate dendritic spine morphology. *Neuron* **47**, 85–100 (2005).
63. W.-Y. Fu, Y. Chen, M. Sahin, X.-S. Zhao, L. Shi, J. B. Bikoff, K.-O. Lai, W.-H. Yung, A. K. Y. Fu, M. E. Greenberg, N. Y. Ip, Cdk5 regulates EphA4-mediated dendritic spine retraction through an ephexin1-dependent mechanism. *Nat. Neurosci.* **10**, 67–76 (2007).
64. Y. Okuyama, K. Umeda, M. Negishi, H. Katoh, Tyrosine phosphorylation of SGEF regulates RhoG activity and cell migration. *PLOS ONE* **11**, e0159617 (2016).
65. S. M. Goebel-Goody, M. Baum, C. D. Paspalas, S. M. Fernandez, N. C. Carty, P. Kurup, P. J. Lombroso, Therapeutic implications for striatal-enriched protein tyrosine phosphatase (STEP) in neuropsychiatric disorders. *Pharmacol. Rev.* **64**, 65–87 (2012).
66. F. Fuentes, D. Zimmer, M. Atienza, J. Schottenfeld, I. Penkala, T. Bale, K. K. Bence, C. O. Arregui, Protein tyrosine phosphatase PTP1B is involved in hippocampal synapse formation and learning. *PLOS ONE* **7**, e41536 (2012).
67. S. Kusakari, F. Saitow, Y. Ago, K. Shibasaki, M. Sato-Hashimoto, Y. Matsuzaki, T. Kotani, Y. Murata, H. Hirai, T. Matsuda, H. Suzuki, T. Matozaki, H. Ohnishi, Shp2 in forebrain neurons regulates synaptic plasticity, locomotion, and memory formation in mice. *Mol. Cell. Biol.* **35**, 1557–1572 (2015).
68. B. Zhang, Y.-L. Du, W. Lu, X.-Y. Yan, Q. Yang, W. Yang, J.-H. Luo, Increased activity of Src homology 2 domain containing phosphotyrosine phosphatase 2 (Shp2) regulates activity-dependent AMPA receptor trafficking. *J. Biol. Chem.* **291**, 18856–18866 (2016).
69. K. Kim, J. Lee, H. Moon, S.-A. Lee, D. Kim, S. Yang, D.-H. Lee, G. Lee, D. Park, The intermolecular interaction of Ephexin4 leads to autoinhibition by impeding binding of RhoG. *Cells* **7**, 211 (2018).
70. K. Kim, J. Lee, S.-A. Lee, H. Moon, B. Park, D. Kim, Y.-E. Joo, D. Park, Intermolecular steric inhibition of Ephexin4 is relieved by Elmo1. *Sci. Rep.* **7**, 4404 (2017).
71. L. Stoppini, P.-A. Buchs, D. Muller, A simple method for organotypic cultures of nervous tissue. *J. Neurosci. Methods* **37**, 173–182 (1991).
72. G. Woods, K. Zito, Preparation of gene gun bullets and biolistic transfection of neurons in slice culture. *J. Vis. Exp.*, e675 (2008).
73. G. F. Woods, W. C. Oh, L. C. Boudewyn, S. K. Mikula, K. Zito, Loss of PSD-95 enrichment is not a prerequisite for spine retraction. *J. Neurosci.* **31**, 12129–12138 (2011).
74. T. A. Pologruto, B. L. Sabatini, K. Svoboda, ScanImage: Flexible software for operating laser scanning microscopes. *Biomed. Eng. Online* **2**, 13 (2003).
75. R. Yasuda, C. D. Harvey, H. Zhong, A. Sobczyk, L. van Aelst, K. Svoboda, Supersensitive Ras activation in dendrites and spines revealed by two-photon fluorescence lifetime imaging. *Nat. Neurosci.* **9**, 283–291 (2006).
76. I. S. Stein, D. K. Park, N. Claiborne, K. Zito, Non-ionotropic NMDA receptor signaling gates bidirectional structural plasticity of dendritic spines. *Cell Rep.* **34**, 108664 (2021).
77. A. S. Leonard, J. W. Hell, Cyclic AMP-dependent protein kinase and protein kinase C phosphorylate *N*-methyl-D-aspartate receptors at different sites. *J. Biol. Chem.* **272**, 12107–12115 (1997).
78. A. S. Leonard, M. A. Davare, M. C. Horne, C. C. Garner, J. W. Hell, SAP97 is associated with the α-amino-3-hydroxy-5-methylisoxazole-4-propionic acid receptor GluR1 subunit. *J. Biol. Chem.* **273**, 19518–19524 (1998).

Acknowledgments: We thank R. Yasuda for providing the FLIM microscope setup design and the custom FLIM software; J. Hell for the GluA1 antibody; and S. Collins, E. Diaz, H. Ho, G. Sell, C. Meyer, M. Alarcon, and L. Lequint for important input and/or critical reading of the manuscript. **Funding:** This work is funded by National Institutes of Health grant numbers: R01 NS06736 and R01 NS137635 (K.Z.), T32 GM007377 (S.P.), T32 MH112507 (S.P.), F31 NS122488 (S.P.), and T32 GM144303 (A.C.). **Author contributions:** Conceptualization: S.P., K.Z., and A.M.H. Methodology: S.P., K.Z., A.C., and A.M.H. Investigation: S.P., A.C., A.M.H, D.S., M.A., and J.C.F. Visualization: S.P. and K.Z. Supervision: K.Z. and S.P. Writing—original draft: S.P. and K.Z. Writing—review and editing: S.P., K.Z., A.C., A.M.H., D.S., M.A., and J.C.F. **Competing interests:** The authors declare that they have no competing interests. **Data and materials availability:** All data needed to evaluate the conclusions in the paper are present in the paper and/or the Supplementary Materials. All raw image files and analysis files are available at Dryad (DOI: 10.5061/dryad.dr7sqvb8b). This study did not generate any code. E5KO mice were obtained from the Greenberg laboratory (*18*).

Submitted 1 April 2024
Accepted 19 February 2025
Published 26 March 2025
10.1126/sciadv.adp5782